OPEN ACCESS
IOP Publishing
Made open access 1 July 2014
Journal of Micromechanics and Microengineering
J. Micromech. Microeng. **24** (2014) 075019 (12pp)
doi:10.1088/0960-1317/24/7/075019

Injection moulding of ultra high aspect ratio nanostructures using coated polymer tooling

J M Stormonth-Darling[1], R H Pedersen[1], C How[2] and N Gadegaard[1]

[1] Division of Biomedical Engineering, School of Engineering, Rankine Building, Oakfield Avenue, University of Glasgow, Glasgow G12 8LT
[2] School of Physics and Astronomy, Kelvin Building, University Avenue, University of Glasgow, Glasgow G12 8QQ

E-mail: Nikolaj.Gadegaard@glasgow.ac.uk

Received 23 February 2014, revised 8 May 2014
Accepted for publication 9 May 2014
Published 23 June 2014

Abstract
Replication-based nanofabrication techniques offer rapid, cost effective ways to produce nanostructured devices for a host of applications in engineering, biological research and beyond. In this work we developed a method to replicate ultra high aspect ratio (UHAR) nanopillars by injection molding with failure rates lower than one pillar in a thousand. We provide a review of the literature in which replication of difficult micro- and nanostructures is facilitated through the use of different tooling materials and surface coatings, before describing the non-adhesive surface coatings which we used to translate a previously developed technique from low to high aspect ratios. This development involved a systematic study of nine different surface coatings on polymer tooling initially patterned by nanoimprint lithography. Using this method we were able to produce injection moulded pillar-like nanostructures with aspect ratios of up to 20:1, more than 6 times that reported elsewhere in the literature for this type of feature.

Keywords: high aspect ratio, injection, moulding, molding, nanopillar, nanoimprint

(Some figures may appear in colour only in the online journal)

1. Introduction

1.1. High aspect ratio nanostructures

Many potential applications of nanostructured surfaces require structures which have aspect ratios (ratio between height and width) that exceed those normally required for general nanofabrication processes such as electronic devices where the thickness each layer of a device tends to substantially less than its lateral dimensions [1]. Despite the fact that it is often technically challenging to build something much taller than it is wide, there are many examples of high aspect ratio (HAR) nanostructures in the literature focused on the pursuit of various applications. Bioinspired non-reflective [2], superhydrophobic [3] and dry adhesive [4] surfaces all require nanostructures with aspect ratios greater than 1:1 and there are also several applications in cell biology research [5–7].

1.2. Injection moulding of nanostructures

Injection moulding is a well established mass production tool for polymeric products of all shapes and sizes which is now drawing the attention of companies and researchers who seek to utilise this high throughput fabrication technique to produce devices with nanoscale dimensions [8]. Much of this research has focussed on the materials which comprise the injection moulder tooling (i.e. the mould itself and particularly its surface) due to limitations on the minimum attainable feature size imposed by the rapid rate at which the injected polymer cools upon contact with the mould surface. Despite being intrinsic to the speed at which replicas can be produced, conventional metallic (usually steel or nickel) tooling conducts the heat away from the molten polymer so quickly that a frozen skin layer forms before it is able to fully fill nanoscale cavities in the mould. Two main schools of thought exist as to how best to

Table 1. Variothermal methods and heat retardant tooling materials used to injection mould micro and nanostructures. A brief summary of tooling performance and highest aspect ratio achieved is provided.

Tooling	Polymer	Performance	Aspect ratio
Variothemal:			
Ni + MEMS heater	PC	Improved, but still incomplete, filling of 320 nm wide, 82 nm deep grooves from 20–60 nm [11, 12].	5.3:1
Steel with 300 Ks^{-1} laser heating	PP	Replication of superhydrophobic conical pillars (5 μm base diameter, non-uniform appearance [13]).	? (appears to be > 2:1)
Ni + electrical induction	COC	Enhanced filling of micro- & nanostructures [14, 15].	9.9:1 (100s of μm)
Electrified Ni	PP	Formation of nanoscale pillars and hair-like structures over 2 minute cycle time [16].	Pillar: 3:1, hair: 300:1.
Steel + Bakelite insulation with steam heating and water cooling	ABS	Defect-free replication of 46 inch LCD panel, heating/cooling contributes over 1 minute to cycle time [17].	N/A (long, flat, thin-walled part)
Heat retardant:			
IR heating + heat resistant polymer layer behind Ni	PMMA	400 nm wide, 600 nm deep channels fully filled with combined variothermal/heat retardant approach [18]	1.5:1
PC with Al or Ti coating	PS	Fill 1–2 μm wide trenches (depth ~100s of nm) to twice the depth achieved by fluorinated Si tooling [19–23].	<1:1
PI + Al coating	PC, PS	Replicated microstructures for over 1000 cycles without damage [20].	<1:1
SU-8 on Ni	COC	Replicated microstructures for over 300 cycles without damage [24].	N/A
PUA + PET	PMMA	Replication of 1–10 μm wide, 10 μm deep gratings [25].	10:1
PVA	COC	Replication of 100 nm pillars, but tooling must be dissolved after each shot [26].	<1:1
PEEK	PP, ABS, PC, COC	Tool wear with some polymers and residue build-up with others, but compatible with PP [27].	4:1
Bulk metallic glass	PMMA	Formation of 100–200 nm bumps [28] and 300 nm ridges [27].	Ridges: 2.8:1, Bumps: <1:1
PI + SU-8	PC	Replication and tuneable stretching of 100 nm pillars for over 1000 cycles [29].	1.4:1

combat this problem. They are variothermal injection moulding and heat transfer retardation techniques. Variothermal techniques use elaborate mechanisms that require the incorporation of plumbing or electrical systems into the construction of the tool, with these additions being used to heat and cool the tooling surface at the appropriate times in order to aid the filling of micro and nanostructures [9, 10]. Heat retardation techniques offer a simpler approach where the tool is made of a thermally insulating material which provides a slower rate of cooling for the polymer, particularly at the mould surface, improving its chances of filling nanoscale cavities before freezing. Table 1 provides a list of tooling solutions found in the literature which have been employed in the replication of micro- and nanostructures by injection moulding where the emphasis of the work has been on the tooling material or method of variothermal implementation. Abbreviations of polymer names in table 1 refer to: poly (carbonate) (PC), poly (propylene) (PP), cyclic olefin copolymer (COC), poly (styrene) (PS), acrylonitrile butadiene styrene (ABS), polyimide (PI), poly (methyl methacrylate) (PMMA), poly (urethane acrylate) (PUA), polyethylene terephthalate (PET), polyvinyl alcohol (PVA) and polyether ether ketone (PEEK).

1.3. Surface coatings

In other replication based micro and nanofabrication techniques, such as hot embossing and nanoimprint lithography (NIL), the addition of non-adhesive surface coatings is a common method used to aid both the filling of moulds and the subsequent demoulding of the replica [30–32]. These have not been explored extensively in the sphere of injection moulding so it is useful to examine the wider literature for evidence of their beneficial effect. In a NIL process surface coatings can greatly improve results through the reduction of surface energies and resulting interfacial friction which occurs at the critical moment when the master and replica are separated [33]. These forces, which are amplified at higher aspect ratios, can lead to the structural failure of features on both the master and moulded or imprinted product [34]. A list of relevant works demonstrating the use of non-adhesive coatings in NIL and injection moulding is provided in table 2.

From these examples, it is clear that non-adhesive surface coatings are a vital addition to any replication based fabrication process, and while fluorosilanes appear to offer a solution in most situations, they may require some optimisation of their composition [31] or prove inferior to metals in some cases [22]. There is probably no one-coating-fits-all solution, but indicative techniques such as water contact angle analysis can guide the way to design and interpret the practical development of potential tooling solutions.

1.4. Summary and outline of the work documented in this paper

The paper documents the development of a technique to facilitate and improve the replication of HAR nanostructures

Table 2. Non-adhesive surface coatings used to enable and enhance replication based micro and nanofabrication techniques. For injection moulding, highest aspect ratios achieved are provided.

Surface coating	Stamp / tooling material	Method	Replica material	Performance	Aspect ratio
Fluorosilanes (FS)	Si / SiO_2	T-NIL/ UV-NIL/ embossing.	Various thermoplastics and curing polymers	Widely regarded as effective non-adhesive coating in replication based fabrication [35–37].	N/A
(NiO,TiO)+FS	Ni	NIL	PMMA	Not as effective as SiO_2+FS [30].	N/A
FS	SU–8	NIL	PMMA, PDMS	High quality replication of multilayer microstructures [38]	N/A
FS	PI	T-NIL / UV-NIL / embossing.	Thermoplastic and UV curing polymers.	Faithful replication on 4 inch wafer [39].	N/A
Nitrided fluorocarbon	SiO_2	NIL	PMMA	Enhanced durability over non-nitrided fluorocarbons [40].	N/A
FS	Si	Injection moulding (IM)	TPU	Protected tooling and enhanced filling of micropillars [41].	2.3:1
FS	Ni	IM	COC	Made it possible to fill sub 100 nm pillars [42].	>2.5:1
FS, MoN, WN	Ni	IM	PC, PMP	Prevented polymer build-up over 1500 cycles with 0.2–1 μm grating [43].	4.5:1
SiOC, diamond-like carbon	brass	IM	PC, ABS	Reduction of demoulding forces by ~40%. Optimum IM conditions are coating/resin specific [44].	1:1
CrN, TiN	Steel	IM	Polyamide with glass fibre	Lower wear to tooling than with traditional methods (heat treatment, Cr deposition, nitriding [45]).	Not patterned
Al,Ti	PC	IM	PS, PC	Better PS filling of microstructures than polymer backplate + SiO_2 + FS [22, 23].	~1:1
Al	PI	IM	PS	Better adhesion reduction after 1000 cycles than uncoated after 100 cycles [20].	~1:1
Au	Ni	IM	PMMA	Resistant to residue [19].	<1:1

by injection moulding. It describes how initial attempts were made to translate a previously developed process [29] from low to high aspect ratio, before incorporating non-adhesive surface coatings to address the limitations of this process. After promising initial results a systematic study was undertaken to evaluate ten potential surface treatments under the criteria of the number of successfully replicated pillars, their height and how straight they were. These results are discussed and the most promising coatings identified. Relevant methods and choice of materials are also discussed.

2. Materials and methods

2.1. Injection moulding

Injection moulding was conducted with PC (Makrolon OD 2015) in an Engel Victory 28 fully hydraulic injection moulding machine (max injection pressure: 2200 bar, max clamping force: 280 kN, max shot volume: 20 cm^3, max injection speed: 52 $cm^3\,s^{-1}$). Given that the very essence of injection moulding is founded in efficiency in an industrial production setting, it was central to the validity of this work that the techniques developed be in line with these values. This is why such an industry standard machine was chosen.

2.2. Tooling

The bulk of the injection moulder tool was comprised of tool hardened steel shaped to produce samples measuring approximately 25 × 25 × 2 mm. One 25 × 25 mm face of the tool contained a frame into which were inserted nanopatterned *inlays* made from a 740 μm thick PI substrate (Cirlex®, Katco UK) covered in 20–40 μm of SU-8 3000 series photoresist (Microchem Corp.) patterned by NIL.

2.3. Fabrication of master for NIL

The master was fabricated from a 25 × 25 × 1 mm quartz. 100 nm diameter circles on a 500 nm pitch were written in PMMA resist by electron beam lithography (EBL) in a Vistec VB6 UHR EWF beam writer. 100 nm of NiCr was deposited on the developed PMMA structure by electron beam evaporation using a Plassys MEB550S metal evaporation tool and lift-off performed in acetone at 50 °C. The HAR nanopillars were formed by transferring the NiCr dot pattern into the quartz substrate by reactive ion etching (RIE) using CHF_3/Ar plasma in an Oxford 80+ RIE dry etch tool. The thickness of the NiCr hardmask was selected for the reason that it allowed slight overetching at each feature's periphery, resulting in sidewall angle of around 5° from the vertical which was required by the subsequent NIL process to reduce friction during demoulding and thereby prevent master failure through pillar breakage. Sidewall angles of this order are often applied to conventional injection moulder tooling in order to improve the release of moulded parts. It was found that masters etched with a more vertical profile suffered from catastrophic pillar breakage during NIL. Interfacial friction during NIL was further reduced by the application of a monolayer of Trichloro(1H,1H,2H,2H-perfluorooctyl)silane (TPFS) to the surface of the master by vapour deposition.

Table 3. List of tooling surface coatings used in this work chosen because of successes reported in the literature.

Coating material(s)	Reason
SiO_2 + TPFS	Ubiquitous in NIL [46, 47] and successful stamp material in this project.
Si_3N_4 + TPFS	Improved durability over SiO_2 + a fluorosilane [40].
Ni + TPFS	Enhanced replication of 40 nm diameter COC pillars compared to Ni alone [42].
Ti	Improved filling of microstructures compared to SiO_2 + a fluorosilane and Al [22].
TPFS only	Improved release of embossed PMMA with fluorinated SU-8 stamp [38].

2.4. Patterning of inlays by NIL

Inlays were fabricated by a refined version of the process developed in an earlier work [29] with the main difference being that the resist was not spin coated, but left as a blob right up until the imprint stage. This amendment, combined with application of the master slowly at an angle, helped to reduce the likelihood of air bubble formation. Specifically, inlay substrates were machined from a sheet of 740 μm thick Cirlex and exposed to O_2 plasma at 200 W for one minute to improve adhesion. A blob of SU-8 3050 measuring approximately 5 mm in diameter was deposited on the substrate directly from the bottle before the sample was softbaked at 100 °C for 2–3 hours to remove solvent content.

Thermal UV NIL was conducted on a hotplate at 96 °C using a custom built apparatus designed to expose the SU-8 through the quartz master with i-line (365 nm wavelength) UV radiation. After the master was slowly lowered face down onto the SU-8 blob, the apparatus was placed on top of the master-substrate assembly and was left for 5 minutes to allow the resist to spread across the substrate and fill all the space between the nanoscale features of the master. The 5 W UV LED inside the NIL apparatus was then switched on for 4 minutes to initiate curing of the SU-8 by simultaneous UV exposure and heating. After this time the apparatus was removed and the sample and substrate were carefully separated with a razor blade. This separation was conducted on the hotplate at imprint temperature to prevent any stress being caused by differences in thermal expansion between the two materials. After NIL inlays were oven baked at 180 °C for 1–3 hours to further harden the SU-8. It was found that the omission of this step would result in cracking of the SU-8 surface during injection moulding.

2.5. Choice of coatings and methods of application

In light of the beneficial effect of surface coatings reported in the literature for injection moulding and other replication based fabrication techniques such as NIL [30], a total of nine distinct non-adhesive coatings were tested alongside an uncoated inlay. These were: Ni, Ti, SiO_2 and Si_3N_4, each with and without an additional TPFS monolayer, as well as TPFS alone. Some coating choices were based on successes reported in the literature. These are briefly summarised in table 3.

Unfluorinated nickel was added to the list due to its widely accepted use as standard injection moulder tooling and uncoated inlays were included as a control. Untreated SiO_2, Si_3N_4 and fluorinated Ti were included to fill in the blanks and ensure that a thorough assessment of the effects of fluorosilane layers on replication performance would be possible. The coatings were applied in a number of ways as detailed in table 4.

2.6. SEM imaging and quantitative assessment of nanostructure replication

Pillar replication success rate was quantified by image analysis of scanning electron microscope (SEM) images of injection moulded samples, sputtered with ~10 nm Au/Pd taken perpendicular to the sample surface (i.e. top-down). Images were thresholded and converted to a black and white binary format before successfully replicated features were counted using ImageJ image analysis software. A feature was considered to be successful if it had sufficient contrast to its surroundings and was not touching or overlapping any of its neighbours (identified by having an area outwith the range 7800 to 50 000 nm^2) as illustrated by figure 1. For each of the four patterned areas, at least three images on two samples (six total, but usually more) were captured. A value of success rate for each image was obtained by dividing the total number of features present by the ideal number that would be visible at that magnification. Mean values were obtained by averaging together the values extracted from each image.

The important thing to consider when interpreting the success rate data is that the stumps produced by replication of broken pillars on the stamp or those with low height due to poor filling will usually appear to be just as successful as perfectly formed pillars, provided there was sufficient feature-background contrast which was usually the case. In these instances it is particularly important to cross reference success rate with height data. Additionally, in the case of pillars leaning to one side, the difference between a success and a failure (a pillar not touching or touching its neighbour) may be the matter of only a few nanometres. Because of this a small amount of variability across one pattern area may lead to large variations in image-to-image success rate.

Circularity data was extracted from the same images as success rate data using results from the same analysis technique with the exception that averages were calculated using the values of all successful features across all images rather than on an image-by-image basis. Circularity used in this way is not an assessment of the actual cross-sectional shape of pillars, but rather an indication of how much the pillar deviates from the z-axis, with a perfectly straight pillar giving a value of 1.0. The fact that circularity data only exists for successful features means that it is more a measure of perfection than success and should be considered as a bonus to any strong combination of height and success rate.

2.7. Analysis by transmission electron microscopy

Transmission electron microscopy (TEM) was used to evaluate the consistency of some types of surface coating after injection moulding had been performed. Inlays were coated

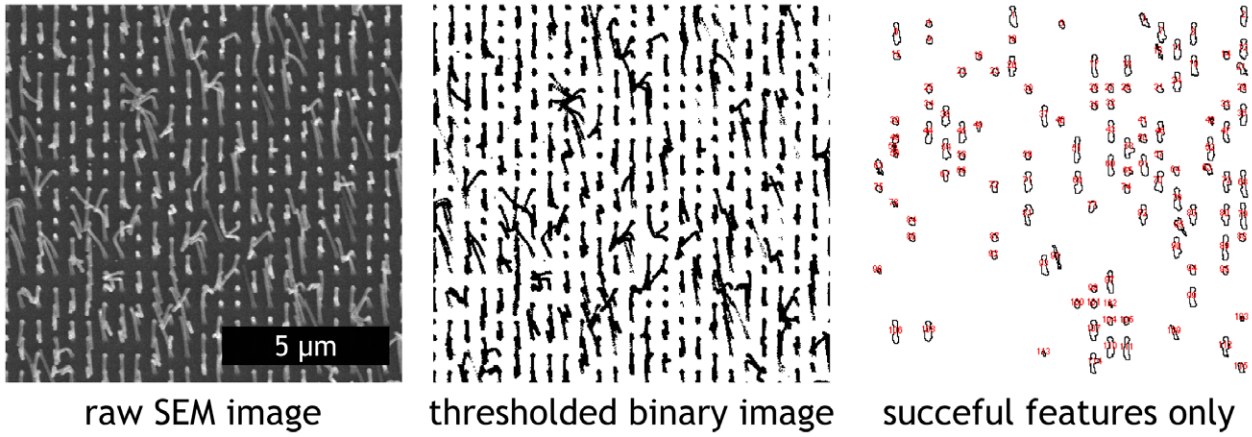

Figure 1. SEM image (left) containing successful and unsuccessful (too large and/or touching a neighbour) features as interpreted by subsequent analysis (centre and right).

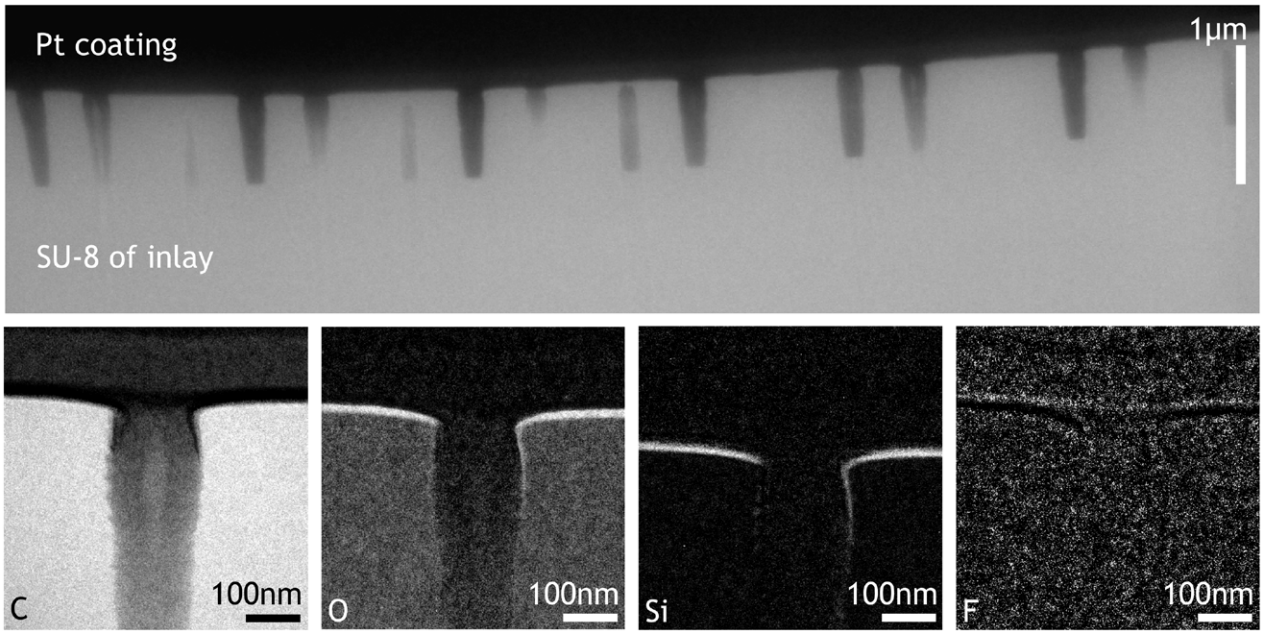

Figure 2. Brightfield TEM overview of SiO2 + TPFS coated inlay (top) and elemental maps of carbon, oxygen, silicon and fluorine included to show the coverage of coatings (bottom). The presence of the specified elements are indicated by bright areas. Si_3N_4 + TPFS coated tooling showed very similar results.

with platinum before thin slices were cut from nanopatterned areas with a focused ion beam (FIB) tool. These sections were examined by TEM to obtain a detailed cross-sectional perspective of the HAR cavities in the inlay and enable elemental mapping to help to determine the coverage of surface coatings.

2.8. Analysis by atomic force microscopy

Pillar height was measured by atomic force microscopy (AFM) across 3 or 5 μm gaps in the pillar array which were included for this purpose. Height was calculated as the difference between the height values of this gap region and the modal height of the peaks of the surrounding pillars. This processing was performed in MatLab. Heights of less than 200 nm were ignored to remove the contribution made by stumps of broken pillars on the master because it was not feasible within a reasonable time frame to locate and take measurements of exclusively 100% defect free areas. Each sample was measured in 4–8 locations and at least two samples produced with each differently coated inlay were measured

3. Results

3.1. Consistency of inlay coatings

TEM analysis of fluorinated SiO_2 and Si_3N_4 coated inlays was conducted after injection moulding work was complete and the inlays had been cleaned by soaking in *N*-Methyl-2-pyrrolidone (NMP) at 50 °C overnight. Figure 2 shows an overview of a slice cut from the SiO_2+TPFS coated inlay accompanied by element maps that reveal information about the coating.

In figure 2 it appears from the overview that HAR holes are only about 60% of the depth that would be expected given

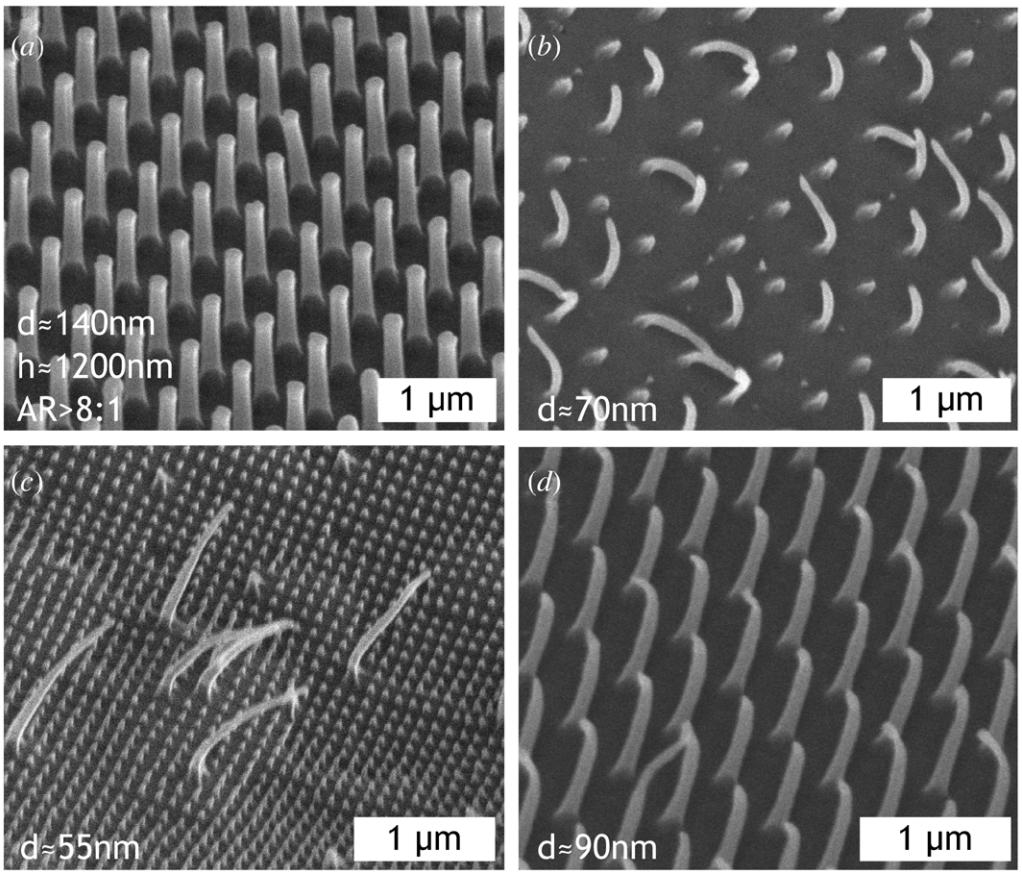

Figure 3. Injection moulded HAR PC nanopillars made without surface coatings. Wider pillars replicate well while thinner ones are less consistent. T_m = 260°C (*a,b,c*) and 280°C (*d*). T_w = 80 °C (*a,c,d*) and 65 °C (*b*). Tilt angle = 30°.

the height of the pillars on the NIL master (975 nm). It is possible that injected polymer accumulated at the bottom of holes and were not cleaned properly due to the cleaning solvents not penetrating sufficiently far down the narrow holes. It is, unfortunately, impossible to tell the difference between the SU-8 of the tooling and the injected PC because their elemental content is so similar. The elemental maps are also highly revealing, indicating that the SiO_2 coating does not penetrate much more than 100 nm down the side of the hole, probably due to the diffusion limiting nature of the geometry. These observations were consistent across all holes examined and Si and N element maps performed on the Si_3N_4 + TPFS inlays showed the same thing. Although this problem was not resolved, the results presented in section 3.3 show that the coatings still made a substantial difference to replication success and pillar height.

3.2. Replication of nanopillars without surface coatings

The first attempts to replicate HAR nanopillars were made without the addition of surface coatings. Some results obtained from these attempts with PC are shown in figure 3. Pillars with diameters of around 140 nm were consistently well formed, but those with diameters of 100 nm and below were not. As shown by the SEM image in figure 3(*c*), sub-100 nm structures either did not fill or were broken off except in cases where four adjacent pillars seemed to coalesce, resulting in wider, highly stretched pillars. This pillar joining was most likely present due to bending/breakage of pillars on the stamp during the patterning of inlays by UV-NIL. Pillars made with moulds originating from a stamp with 100 nm diameter features were highly inconsistent and thinned by stretching at melt temperature (T_m) = 260°C and tool temperature (T_w) = 65°C (figure 3 (*b*)) and were slightly thinned with a slight bend and tails at the tips when moulded at T_m/T_w = 280/80°C (figure 3(*d*)).

Furthermore, the larger pillars have a clearly defined tip which exceeds the width of main bulk of the pillar; a phenomenon that was also observed with the results from coated inlays and is discussed during the analysis of those results below. Through this scoping exercise we identified the ~100 nm diameter size range as an area of promise where replication quality and consistency might be improved by the introduction of non-adhesive coatings on injection moulder tooling.

3.3. Replication of nanopillars with surface coatings

In initial production runs using inlays coated in TPFS only as well as fluorinated SiO_2 and Si_3N_4, high levels of successful features were achieved at several different tool/melt temperature combinations as indicated by the bar graph in figure 4. These results show that all but one of these fluorinated coatings facilitated the successful replication of close to 95% or higher of HAR nanopillars with PC. Fluorinated SiO_2 seemed to perform the best overall with a value of

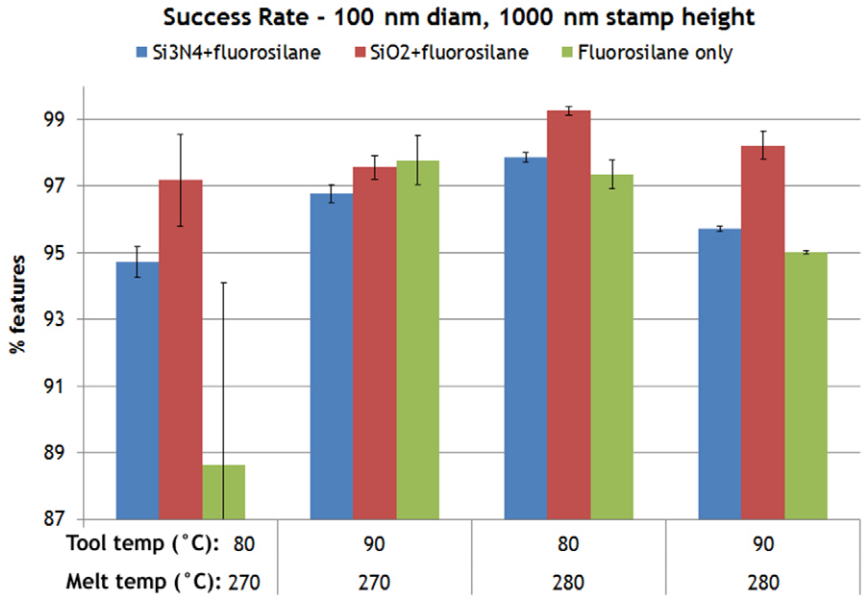

Figure 4. Success rate of injection moulded PC nanopillars made with three differently coated inlays at four different temperature conditions. v_i = 50 cm3s-1, t_c = 5 s.

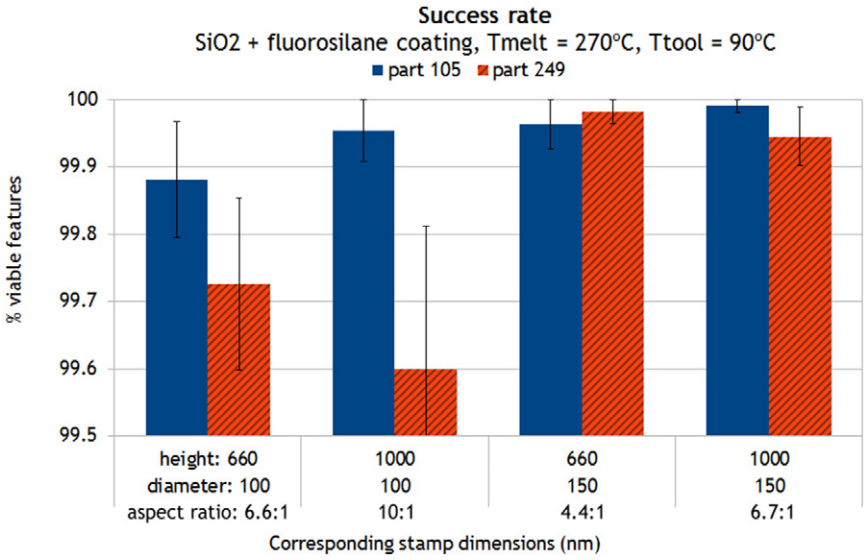

Figure 5. Success rate of HAR nanopillars of different sizes for the 105th and 249th parts produced in the same production run. T_m = 270 °C, T_w = 90 °C, v_i = 50 cm^3s^{-1}, t_c = 5 s.

over 99% achieved for standard PC moulding conditions of T_w/T_m = 80/280 °C.

Consistently high success rates were also achieved with pillars of four distinct dimensions at one temperature combination (T_w/T_m = 90/270 °C) using only SiO_2 coated tooling as indicated in figure 5. In these results, pillars with designed aspect ratios between ~4:1 and 10:1 were replicated with a success rate of over 99.5% in all cases over the course of 249 injection moulder cycles. SEM imaging, however, shows that pillars were consistently and uniformly stretched to twice their designed height, yielding aspect ratios of over 20:1 as shown in figure 6. In light of nanopillar achievements reported elsewhere in the literature, it is quite remarkable to achieve aspect ratios of 20:1 especially with a pillar failure rate of less than one in a thousand. It is noteworthy, however, that the pillars with smaller diameter show a decrease in success rate between the 105th and 249th cycle which is statistically significant at the highest aspect ratio.

In light of the promising results shown above, a systematic study was undertaken to assess the performance of 9 different types of tooling coating at two different temperature combinations (T_w/T_m = 65/260 °C and 80/280 °C) which were chosen because they were the values which corresponded to minimal/maximal stretching in an earlier work [29]. Nanopillar replication was measured in terms of the same success rate metric used above as well as the heights of the replicated HAR nanopillars and the circularity of these features when viewed from above (i.e. how straight they are). Injection speed (v_i) and cooling time (t_c) were kept constant at 50 cm^3s^{-1} and 15 s respectively. The 15 s cooling time was chosen so that the PC

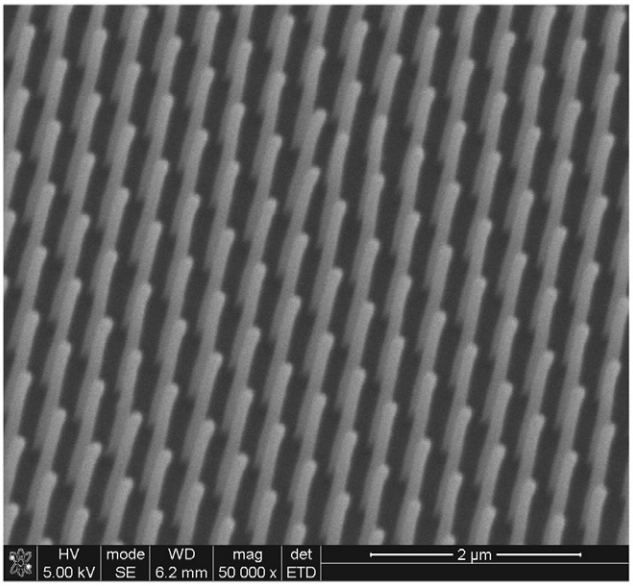

Figure 6. SEM image of PC nanopillars with aspect ratio 20:1 (diameter = 0.1 μm, height = 2 μm) produced by injection moulding with SiO2+TPFS coated inlays (T_m =270 °C, T_w = 90 °C, v_i = 50 cms^{-1}, t_c = 5 s). Viewing angle = 30°.

should be well below T_g at the point of ejection, based on simulation data (supplementary information) which shows that nanopillars should be below T_g after 8 s and the bulk of the part should follow after about 10.5 s.

Figure 7 shows how these 9 types of coating and uncoated tooling performed in terms of the three metrics of height (normalized to pillar height on master), success rate and circularity. Representative SEM images of injection moulded PC pillars are provided to show the morphology of typical pillars replicated using different tooling coatings with lines indicating which coating was used.

4. Discussion

Looking firstly at the SEM images in figure 7 some excellent results have been obtained in terms of the formation of HAR nanopillars and several unsuitable coatings have been exposed such as fluorinated nickel which gives strange curled pillars (figure 7(*g*)). Although none of the replicated pillars closely resemble the pillars on the stamp (figure 8, right), some come close (such as SiO_2-only and Ni at T_m/T_w = 260/65 °C, uncoated at T_m/T_w = 280/80 °C and Ti only at both temperature combinations – figure 7(*a, c, i, h* and *l*) respectively) and many of them are very straight and regular and appear to be substantially taller than on the original quartz master. These apparently stretched pillars, such as those in figure 7(*b, d, e, f, h, i, j, k, m, n* and *p*), tend to have a well-defined tip (circled in figure 8, bottom right) which is presumably the location where the base of the mould cavity "*grips*" the polymer, causing stretching of the main bulk of the pillar to stretch as the part is ejected. This effect was previously observed in the experiments documented in an earlier work [29] and in the initial experiments without coatings in this paper. The probable cause of this gripping action is illustrated in figure 8 and is probably the result of increased friction due the lack of a non-adhesive coating at the base of the inlay's HAR nanopits as indicated by the TEM data (figure 2). Also evident are instances of substantial pillar-to-pillar variation (figure 7(*a, e* and *n*)) which is discussed in more detail below.

Turning the attention to the graphical data in figure 7, perhaps the most noticeable thing is the effect of temperature on height. This is consistent with previous findings [29] where the increased temperatures made it possible for injection moulded nanopillars to exceed the height of the original quartz stamp by a controlled stretching process. In contrast to those lower aspect ratio pillars (~1:1) which would be fully filled using an uncoated inlay at 260/65 °C, these high aspect ratio structures will not fill beyond around 200 nm (~0.2 normalized) at that temperature combination nor much above 600 nm (~0.6 normalized) with the higher temperatures without the presence of a non-adhesive surface coating. Whether this is due to polymer build-up at the base of holes or just incomplete filling, it is clear that non-adhesive surface coatings are required to fully replicate HAR nanopillars.

In terms of success rate, perhaps more important than height, values above 90% are only seen for the non-fluorinated metal coatings. It is to be expected that Ni and Ti will not facilitate the binding of a TPFS layer because the chemistry does not provide a stable covalent bond to the surface. Additionally, the HCl produced in the fluorination reaction will react with the metal oxide to produce a chemistry that could explain the poor replication performance in both cases. Furthermore, both varieties of unfluorinated metal fail to facilitate full replication of pillar heights (although nickel comes close) and they have displayed problems of polymer build-up and/or surface damage (supplementary data) which make them unsuitable for the fabrication of usable devices. In general it seems as though TPFS-only and the fluorinated oxide and nitride coatings are the most promising, but substantial refinement would be required to achieve a near 100% success rate and uniform height, before even beginning to consider attempting to perfect the straightness of pillars as measured by circularity.

From direct observation of injection moulded parts produced it is possible to explain some of the variation in the data as highlighted by the error bars in figure 7. This variation appears to occur on three distinct levels: sample-to-sample variation, millimetre/micrometre scale variation and pillar-to-pillar variation.

The method by which success rate was measured highlights image-to-image (micrometre/millimetre scale) variability on samples where pillar bending was near the success/failure threshold of a pillar touching its neighbour. Due to the method of characterisation, a small yet critical difference in pillar bending between two images could see one have a close to maximal success rate and the other obtain success rate of zero. Locations on the dataset overview figures with relatively large error bars for success rate may be candidates for this type of variation if they are accompanied by a relatively low value for circularity such as Si_3N_4 only, SiO_2 only, SiO_2 +TPFS and Ti+TPFS at 280/80 °C. In the case of SiO_2 + TPFS, for example, the success rate error bars are around 20% of the mean value and a non-straight morphology is indicated by a circularity of below 0.7, so the fact that the mean height is

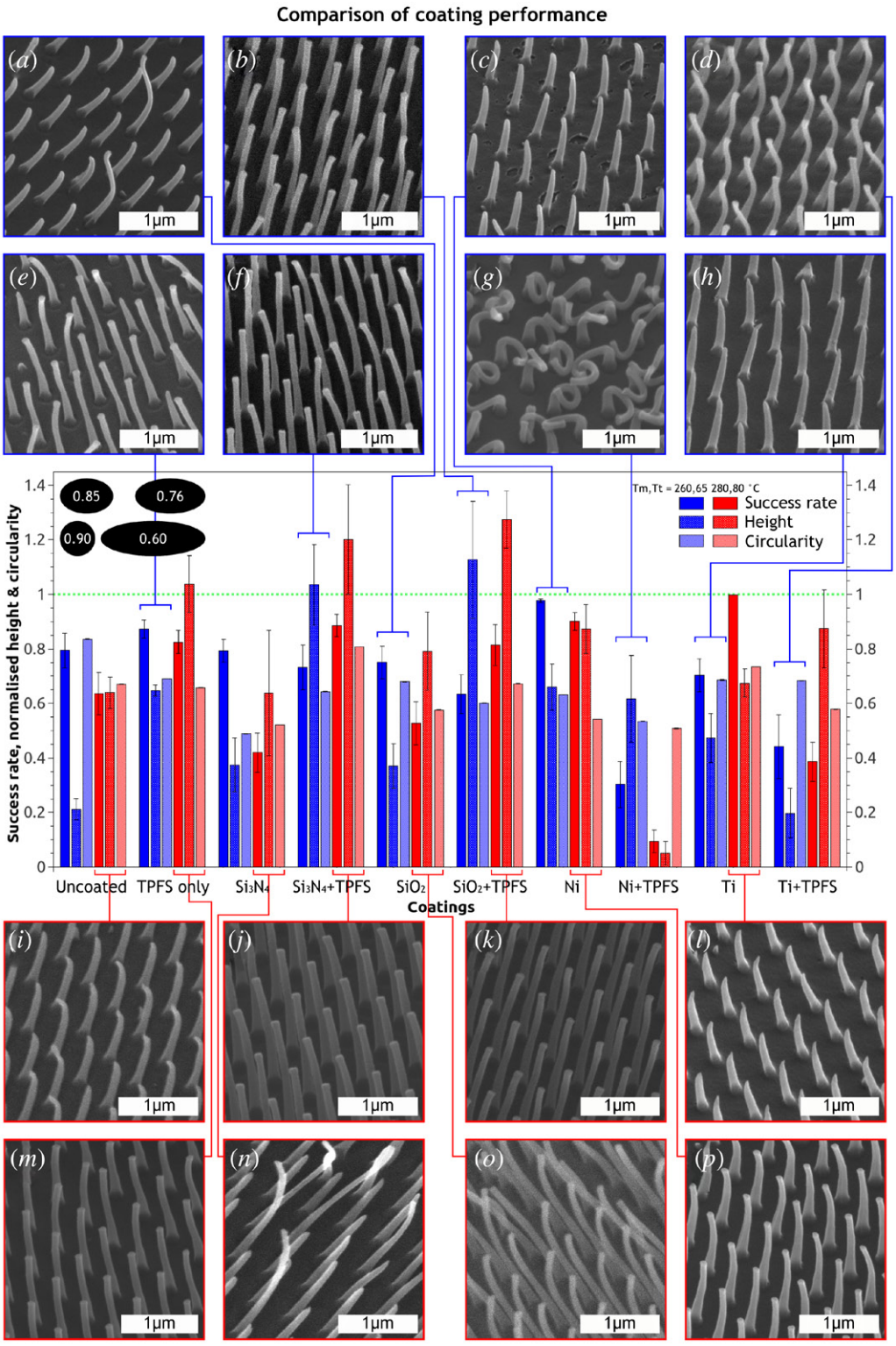

Figure 7. Success rate, normalized height and circularity of nanopillars made with different surface coatings with selected corresponding SEM images. Viewing angle = 30°. A visual reference for circularity is provided in the top left corner of the graph.

greater than that of the stamp suggests that many of these tall pillars were indeed bending to the extent of failure in terms of the criteria for success rate. Without knowing the consistency of coatings over a surface it is possible to call this into question as a possible cause of variability across a sample at the millimetre scale. Although metal evaporation, CVD and ICP deposition are specifically designed to deliver highly uniform layers, the layers they provide are not designed to for the large physical forces subjected to injection moulder tooling. With layers as thin as 10 nm it is not unreasonable to suggest that under injection moulding conditions any weakness in integrity could be readily exacerbated.

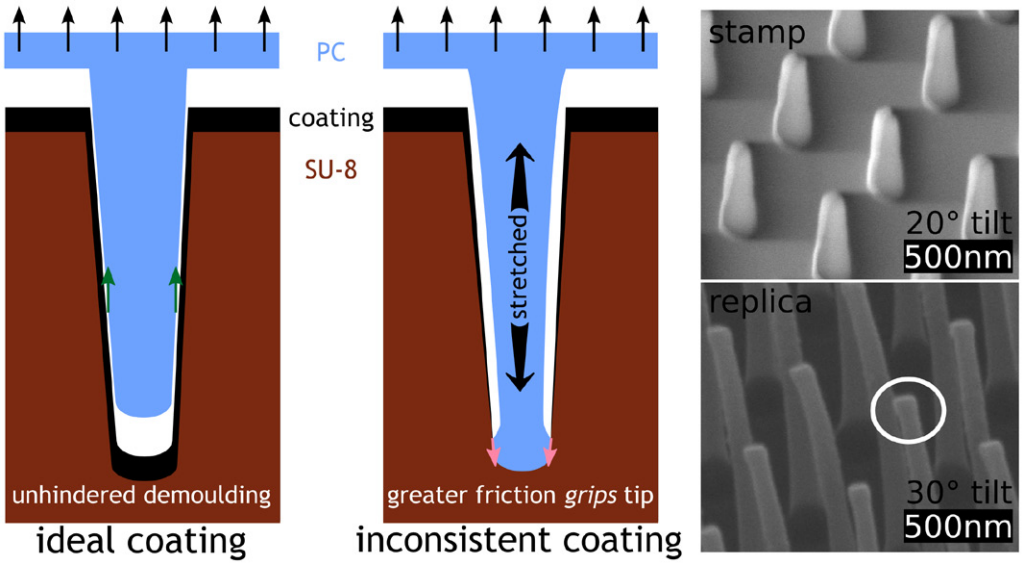

Figure 8. Schematic diagram of pillar stretching due to inconsistent coating and SEM images showing difference in pillar morphology between original quartz stamp and a typical stretched PC replica.

Table 4. Methods of application and thicknesses of tooling coatings used in this work.

Coating	Thickness (nm)	Method of deposition
Si_3N_4	10	ICP deposition
SiO_2	10–15	PECVD
Ni	10–12	Electron beam evaporation
Ti	10–12	Electron beam evaporation
TPFS	monolayer	Vapour deposition

Variation on the pillar-to-pillar scale is difficult to quantify due to the vast amount of images that would have to be captured in a systematic way and the many parameters that would have to be interpreted by computer analysis. Large volume image processing and machine learning techniques such as those used in, for example, cell biology [48] could be incorporated here, but the amount of SEM time and difficulty of automating an SEM to perform the necessary measurements make such analysis beyond the scope of this project. A likely cause of this type of variation is the consistency of surface coatings on the sub feature size scale, particularly towards the bottom of high aspect ratio cavities in the inlays. This, or a physical deformation at the same location, could increase the friction between the polymer and tooling at the pillar tip, causing it to be stretched more than its neighbours when the part is demoulded. Indeed, it may be a consistent occurrence of such physical inconsistencies that cause the more uniform formation of pillars which exceed the height of those on the stamp (such as those in figure 7(*b, f, j, k, m* and *p*) which refer mainly to fluorinated oxide and nitride as well as nickel and TPFS-only at T_m/T_w = 280/80 °C). The TEM data obtained, such as that presented in figure 2, would suggest that poor coverage of coatings within holes is a common occurrence.

In comparing the results of the systematic study (figure 7) to those of the smaller ones (figure 4 and figure 5) there is a clear and major discrepancy between them in terms of the success rates achieved. On very important factor that could explain this is cooling time (t_c). For the two datasets immediately above, t_c was set to 5 s, but in the large study t_c was set to 15 s to ensure that the PC would definitely be below T_g. This was based on the simulations presented in the supplementary data which state that the temperature of a 1 μm tall 100 nm diameter pillar should fall below T_g about 8 s after injection when using our Cirlex/SU-8 inlays (compared to ~10^{-8} s when using nickel inlays). Despite the fact that cooling time did not appear to play a significant role in the earlier work with low aspect ratio pillars [29], it may be that it does here and/or that the simulation is providing false information about the time at which the PC comprising the newly formed pillars solidifies. Indeed it is hard to think of a way that the pillars could stretch without being above T_g, because in their solid state a pulling force at the tip would most likely cause them to snap. If the simulation is incorrect, then the consistency of the two small studies conducted with t_c = 5 s could be attributed to uniform pillar stretching, while the large study could be displaying its inconsistencies because t_c = 15 s is a critical time point in the cooling process where pillar temperatures are very close to T_g and small local variations could cause adjacent pillars/regions to be slightly above and below T_g at the point of ejection. A systematic study of cooling time was not pursued because the formation of ultra high aspect ratio (UHAR) nanostructures was successfully achieved, but it would certainly be an interesting parameter to explore in a future extension of this work.

Despite significant variation within the measurements there are some encouragingly high success rates which accompany heights greater than or equal to that of the stamp. These are particularly prevalent with the higher temperature combination with the fluorinated oxide and nitride coatings and, to a lesser extent in terms of height, the non-fluorinated metal coatings. The fluorinated oxide and nitride do not surprise in this regard in light of the promising water contact angle (WCA) and x-ray photon spectroscopy (XPS) results (supplementary data), but the metals raise some questions, particularly given the residue/damage observed (supplementary data). Nickel is well established as a successful tooling material for injection moulding nanopatterns

when the features are holes and titanium has been the basis of a recent patent on similar hybrid tooling to that developed in this project [23]. Perhaps these materials require a base level of polymer residue accumulation to provide a favourable surface interaction and may be less prone to damage and bulk residue build up if they existed as something more substantial than a 10 nm layer. It is clearly evident that attempts to apply fluorosilane coatings to either of them have a negative effect on their ability to replicate nanostructures so there may well be a chemistry component to this which has not been considered. Whatever the case may be, the residue/damage shown in supplementary data makes them unfit to be applied to this particular tooling solution where they could not exist as anything other than a thin (< 20 nm) film without obscuring the nanopattern.

5. Conclusions

A polymer-based heat retardant tooling solution developed in a previous work [29] has been successfully translated to enable the fabrication of UHAR PC nanopillars with diameters of 100 nm and aspect ratios of 10:1 and higher. The realisation of these features does however fall sort of true *replication* given the stretched morphologies of the injection moulded pillars which do not really resemble those on the stamp. The consistency of pillar height, success rate and circularity seems to be a major issue as shown by the large dataset, but the two smaller studies (figure 4 and figure 5) indicate a much higher consistency for success rate (> 99.5%). These discrepancies may be attributable to differences in cooling time, but further investigation would be required to confirm this.

Inlay coatings have been shown to affect height, success rate and circularity of UHAR PC nanopillars even though they may not penetrate all the way to the bottom of negative features in the tooling. While there were inconsistencies across the entire coating study there were clearly coatings which outperformed the others; namely: TPFS-only, SiO_2+TPFS, Si_3N_4+TPFS, Ni-only and Ti-only (figure 7). Of these five, the fluorinated coatings seemed to excel more at stretching at the expense of success rate (although this was still generally above 80% at the higher temperature conditions), while the metal coatings might not fully fill UHAR structures, but they tended to have close to 100% success rate. In light of this and the > 93% success rates obtained for fluorinated oxide and nitride and the TPFS-only inlays (figure 4 and figure 5), it would seem that all five have good potential, but the three fluorinated coatings may offer the greatest potential for achieving higher aspect ratios if the heights can be made more consistent. These three also seemed to show promise in terms of the durability metrics of WCA and XPS (supplementary data) and the consistent success rate of SiO_2+TPFS up to 249 shots (figure 5) is encouraging. Inaccurate replication may be partially explained by the failure of SiO_2 and Si_3N_4 coatings to cover the interior of holes in tooling as revealed by TEM analysis (figure 2), but the fact that different coatings still affected performance indicates that this is only part of the cause and may not be the norm in all cases.

Potential applications of UHAR nanostructures were not directly implemented, although it is likely that most of the structures produced would exhibit hydrophobic properties if water droplets remain in the heterogeneous wetting state where they only touch the tips of nanopillars. It is also feasible that dry adhesive hair-like structures and non-reflective structures could be realised if a suitable stamp can be fabricated and HAR pillar stretching can be prevented or selectively encouraged as required. Indeed, a future extension of this work could well include attempts to implement structures for particular applications such as these, but a systematic study into the effects of tool/melt temperature conditions and a solution to the problem of coating conformity should precede this to improve results with the present structures and ease the development of new ones.

This work has documented the successful fabrication of UHAR nanopillars by injection moulding with varying degrees of success and characterized a wide range of parameters that can affect the outcome of this fabrication technique. We have shown that it is possible to mass produce nanopillars with aspect ratios of more than 20:1with success rates of almost 100% as well as revealing areas where inconstancies can arise and identified cooling time and coating uniformity as avenues for future investigation. Furthermore, we have established methods with which to analyse future results and optimise the technique so that injection moulding with heat retardant polymeric tooling may become an established member of the family of high throughput replication based nanofabrication techniques.

Acknowlegements

The authors would like to acknowledge the help and support of technical staff and other researchers at the James Watt Nanofabrication Centre and mechanical workshop at the University of Glasgow, as well as the assistance of Mr William Smith of the School of Physics and Astronomy for TEM substrate preparation. This work was partially funded by an EPSRC Doctoral Training Allowance and the EC funded NaPANIL project (Contract No. FP7-CP-IP 214249-2).

References

[1] Chen Y and Pepin A 2001 Nanofabrication: conventional and nonconventional method *Electrophoresis* **22** 187–07
[2] Brunner R, Sandfuchs O, Pacholski C, Morhard C and Spatz J 2012 Lessons from nature: biomimetic subwavelength structures for high-performance optics *Laser Photonics Rev.* **6** 641–59
[3] Wang J D, Chen H S, Sui T, Li A and Chen D R 2009 Investigation on hydrophobicity of lotus leaf: experiment and theory *Plant Sci.* **176** 687–95
[4] Jeong H E and Suh K Y 2009 Nanohairs and nanotubes: Efficient structural elements for gecko-inspired artificial dry adhesives *Nano Today* **4** 335–46
[5] Padeste C, Özçelik H, Ziegler J, Schleunitz A, Bednarzik M, Yücel D and Hasırcı V 2011 Replication of high aspect ratio pillar array structures in biocompatible polymers for tissue engineering applications *Microelectron. Eng.* **88** 1836–39
[6] Ghassemi S, Biais N, Maniura K, Wind S J, Sheetz M P and Hone J 2008 Fabrication of elastomer pillar arrays with modulated stiffness for cellular force measurements *J. Vac. Sci. Technol.* B **26** 2549–53

[7] Fu J, Wang Y k, Yang M T, Desai R A, Yu X, Liu Z and Chen C S 2010 Mechanical regulation of cell function with geometrically modulated elastomeric substrates *Nat. Methods* **7** 733

[8] Yang C, Yin X H and Cheng, G M 2013 Microinjection molding of microsystem components: new aspects in improving performance *J. Micromech. Microeng*. **23** 093001

[9] Yao D and Kim B 2002 Development of rapid heating and cooling systems for injection molding applications *Polym. Eng. Sci.* **42** 2471–81

[10] Chang P C and Hwang S J 2006 Experimental investigation of infrared rapid surface heating for injection molding *J. Appl. Polym. Sci*. **102** 3704–13

[11] Kim Y, Cho Y and Kang S 2005 Replication of high density optical disc using injection mold with MEMS heater *Microsyst. Technol*. **11** 464–69

[12] Michaeli W and Klaiber F 2009 Development of a system for laser-assisted molding of micro- and nanostructures *J. Vac. Sci. Technol.* B **27** 1323–26

[13] Bekesi J, Kaakkunen J J J, Michaeli W, Klaiber F, Schoengart M, Ihlemann J and Simon P 2010 Fast fabrication of super-hydrophobic surfaces on polypropylene by replication of short-pulse laser structured molds *Appl. Phys. A-Matter*. **99** 691–95

[14] Park K and Lee S I 2010 Localized mold heating with the aid of selective induction for injection molding of high aspect ratio micro-features *J. Micromech. Microeng.* **20** 035002

[15] Kim S, Shiau C S, Kim B H and Yao D 2007 Injection molding nanoscale features with the aid of induction heating *Polym-Plast. Technol*. **46** 1031–37

[16] Yoo Y E *et al* 2009 Injection molding of a nanostructured plate and measurement of its surface properties *Curr. Appl Phys.* **9** e12–e18

[17] Wang G, Zhao G, L H and Guan Y 2009 Research on a new variotherm injection molding technology and its application on the molding of a large LCD panel *Polym-Plast. Technol.* **48** 671–81

[18] Lin H Y, Chang C H and Young W B 2011 Experimental study on the filling of nano structures with infrared mold surface heating *Int. Polym. Proc*. **26** 73–81

[19] Yoon S H, Palanisamy P, Padmanabha P, Mead J L and Barry C M F 2009 Comparison of tooling materials in injection molding of microscale features *Proc. ASME Int. Mech. Eng. Cong. and Expo. (Lake Buena Vista, FL; Nov. 2009)* pp 545–52

[20] Kim Y, Yoon S H, Lee J S, Johnston S, Mead J L and Barry C M F 2010 Performance of hybrid tooling in micro injection molding *Proc. Ann. Tech. Conf. Soc. Plast. Eng*

[21] Yoon S H, Lee J, Park K, Mead J L, Matsui S and Barry C M F 2006 Critical factors for nanoscale injection molding *Proc. SPIE.* **6380** 63800k-1

[22] Yoon S H, Padmanabha P, Lee J S, Mead J L, Barry C M F, Cha N G, Busnaina A A and Park K 2008 Evaluation of metal-polymer hybrid tooling for micro-injection moulding *Proc. Ann. Tech. Conf. Soc. Plast. Eng (Milwaukee, WI)*

[23] Yoon S H, Barry C M F, Mead J L, Cha N G and Busnaina A A (University of Massachusetts Lowel, Northeastern University) 2011 Methods for forming metal-polymer hybrid tooling for forming parts having micro features *US Patent* US20110123711 A1

[24] Hansen T S, Selmeczi D and Larsen N B 2010 Fast prototyping of injection molded polymer microfluidic chips *J. Micromech. Microeng*. **20** 015020

[25] Park S H, Lee W I, Moon S N, Yoo Y E and Cho Y.H 2011 Injection molding micro patterns with high aspect ratio using a polymeric flexible stamper *Express Polym. Lett*. **5** 950–58

[26] Kim S H, Jeong J H and Youn J R 2010 Nanopattern insert molding *Nanotechnology* **21** 205302

[27] Griffiths C A, Bigot S, Brousseau E, Worgull M, Heckele M, Nestler J and Auerswald J 2010 Investigation of polymer inserts as prototyping tooling for micro injection moulding *Int. J. Adv. Manuf. Tech.* **47** 111–23

[28] Zhang N, Byrne C J, Browne D J and Gilchrist M D 2012 Towards nano-injection molding *Mater. Today* **15** 216–21

[29] Stormonth-Darling, J M and Gadegaard N 2012 Injection moulding difficult nanopatterns with hybrid polymer inlays *Macromol. Mater. Eng*. **297** 1075–80

[30] Park S, Schift H, Padeste C, Schnyder B, Kotz R and Gobrecht J 2004 Anti-adhesive layers on nickel stamps for nanoimprint lithography *Microelectron. Eng*. **73–4** 196–01

[31] Schift H, Saxer S, Park S, Padeste C, Pieles U and Gobrecht J 2005 Controlled co-evaporation of silanes for nanoimprint stamps *Nanotechnology* **16** S171–75

[32] Schulz H, Osenberg F, Engemann J and Scheer H C 2000 Mask fabrication by nanoimprint lithography using anti-sticking layers *Proc. SPIE* **3996** 244–49

[33] Guo Y H, Liu G, Zhu X L and Tian Y C 2007 Analysis of the demolding forces during hot embossing *Microsyst. Technol*. **13** 411–15

[34] Matschuk M, Bruus H and Larsen N B 2010 Nanostructures for all-polymer microfluidic systems *Microelectron. Eng*. **87** 1379–82

[35] Beck M, Graczyk M, Maximov I, Sarwe E L, Ling T G I, Keil M and Montelius L 2002 Improving stamps for 10 nm level wafer scale nanoimprint lithography *Microelectron. Eng*. **61–2** 441–48

[36] Park S, Padeste C, Schift H and Gobrecht J 2003 Nanostructuring of anti-adhesive layers by hot embossing lithography *Microelectron. Eng* **67–68** 252–58

[37] Guo L J 2007 Nanoimprint lithography: methods and material requirements *Adv. Mater*. **19** 495–13

[38] Moresco J, Clausen C H and Svendsen W 2010 Improved anti-stiction coating of SU-8 molds *Sensor Actuat B-Chem.* **145** 698–01

[39] Wu C C, Hsu S L C and Lo I L 2010 Fabrication and Application of Polyimide Plastic Molds for Nanoimprint Lithography *J. Nanosci. Nanotechnol*. **10** 6446–52

[40] Kim H H, Park S G, Lee E H, Lee S G and O B H 2011 Durability of nitrided fluorocarbon polymer films for nanoimprint lithography *Thin Solid Films* **519** 5490–93

[41] Yoon S H, Cha N G, Lee J S, Park J G, Carter D J, Mead J L and Barry C M F 2010 Effect of processing parameters, antistiction coatings, and polymer type when injection molding microfeatures *Polym. Eng. Sci.* **50** 411–19

[42] Matschuk M and Larsen N B 2013 Injection molding of high aspect ratio sub-100 nm nanostructures *J. Micromech. Microeng*. **23** 025003

[43] Miikkulainen V, Suvanto M, Pakkanen T A, Siitonen S, Karvinen P, Kuittinen M and Kisonen H 2008 Thin films of MoN, WN, and perfluorinated silane deposited from dimethylamido precursors as contamination resistant coatings on micro-injection mold inserts *Surf. Coat. Technol*. **202** 5103–09

[44] Griffiths C A, Dimov S S, Brousseau E B, Chouquet C, Gavillet J and Bigot S 2010 Investigation of surface treatment effects in micro-injection-moulding *Int. J. Adv. Manuf. Tech*. **47** 99–10

[45] Cunha L, Andritschky M, Pischow K, Wang Z, Zarychta A, Miranda A S and Cunha A M 2002 Performance of chromium nitride and titanium nitride coatings during plastic injection moulding *Surf. Coat. Technol*. **153** 160–65

[46] Park S, Schift H, Padeste C, Schnyder B and Gobrecht J 2004 Improved anti-adhesive coating for nanoimprint lithography by co-evaporation of fluorinated mono- and trichlorosilanes *Nontraditional Approaches to Patterning* ed S Yang, Y Xia, J Liu and C D E Lakeman (Materials Research Society) pp 37–39

[47] Schift H 2008 Nanoimprint lithography: an old story in modern times? a review *J. Vac. Sci. Technol.* B **26** 458–80

[48] Reynolds P M, Pedersen R H, Stormonth-Darling J, Dalby M J, Riehle M O and Gadegaard N 2013 Label-free segmentation of co-cultured cells on a nanotopographical gradient *Nano Lett*. **13** 570–76